Springer

Journal of
Mechanical
Science and
Technology

Journal of Mechanical Science and Technology 22 (2008) 639~646

www.springerlink.com/content/1738-494x

Nodeless variable finite element method for stress analysis using flux-based formulation

Sutthisak Phongthanapanich[1] and Pramote Dechaumphai[2,*]

[1]*Department of Mechanical Engineering Technology, College of Industrial Technology, King Mongkut's University of Technology North Bangkok, Bangkok 10800, Thailand*

[2]*Mechanical Engineering Department, Chulalongkorn University, Bangkok 10330, Thailand*

(Manuscript Received April 3, 2007; Revised December 20, 2007; Accepted January 2, 2008)

Abstract

A nodeless variable element is combined with an adaptive meshing technique to improve solution accuracy of the finite element method for analyzing two-dimensional elasticity problems. The nodeless variable element employs quadratic interpolation functions to provide higher solution accuracy without requiring additional actual nodes. The flux-based formulation is developed for the nodeless variable finite element to reduce the complexity in deriving the finite element equations as compared to the conventional finite element method. The superconvergent patch recovery procedure is implemented to compute accurate stresses from the nodeless variable finite element solutions. The effectiveness of the combined procedure for providing higher solution convergence rate from the proposed formulation is evaluated by two well-known examples.

Keywords: Nodeless variable finite element method; Flux-based formulation; Adaptive mesh; Stress analysis

1. Introduction

Prediction of accurate structural responses induced by both the mechanical and thermal loads is important in the design of many structures. The finite element method has been used as a tool to predict the response of aerospace structures caused by the thermal effect, as well as the critical stresses on vehicle components due to a combination of different load inputs [1-3]. In the prediction of the stress solution, a conventional finite element formulation with standard finite element types has been frequently employed. The solution accuracy was improved by applying the *h*-, *p*-, *hp*- or *r*-versions of finite element analysis [4-7]. The objective of this paper is to develop a procedure to improve the predicted stress distribution by using an alternative finite element method. The nodeless variable finite element previously developed for heat transfer analysis [8] is extended for the stress analysis in this paper in order to increase the accuracy of the predicted displacement and stress solutions. The nodeless variable finite element uses quadratic interpolation functions to describe the displacement distribution over the element without requiring additional actual nodes. The paper also introduces and implements a flux-based formulation to derive the finite element matrices for such nodeless variable element. The flux-based formulation can simplify the finite element computational procedure as compared to the conventional finite element method.

To further improve the structural analysis solution accuracy, an adaptive unstructured meshing technique [5] is also incorporated. Such technique was first designed for analyzing hyperbolic problems, and has been modified recently for solving both elliptic as well as parabolic problems. Finally, the superconvergent patch recovery procedure [9] is modified for the nodeless variable finite element to improve the predicted stress solutions. The effectiveness of the com-

*Corresponding author. Tel.: +66 0 2218 6610
E-mail address: fmepde@eng.chula.ac.th
DOI 10.1007/s12206-008-0102-9

bined procedure for providing higher rate of the solution convergence is demonstrated by two examples: (1) a large plate with a small circular hole subjected to unidirectional tensile load, and (2) a short cantilever beam with a rigidly fixed side.

2. Finite element structural analysis

2.1 Governing equations and boundary conditions

Two-dimensional structural response is governed by the equilibrium equations that can be written in conservation form as,

$$\frac{\partial\{E_S\}}{\partial x}+\frac{\partial\{F_S\}}{\partial y}=0 \tag{1}$$

where the flux vector components $\{E_S\}$ and $\{F_S\}$ contain the stress components given by,

$$\{E_S\}=\begin{Bmatrix}\sigma_{xx}\\ \sigma_{xy}\end{Bmatrix} \text{ and } \{F_S\}=\begin{Bmatrix}\sigma_{xy}\\ \sigma_{yy}\end{Bmatrix} \tag{2}$$

The stress components σ_{xy}, σ_{yy} and σ_{xy} are related to strain components by Hooke's law,

$$\{\sigma\}=[C]\{\varepsilon\} \tag{3}$$

where $\{\sigma\}$ is the vector of the stress components, $[C]$ is the matrix of the material elastic constants, and $\{\varepsilon\}$ is the vector of the strain components.

These equations are to be solved with the boundary conditions that may consist of (1) the specified displacements, u and v, in the x- and y-directions, respectively,

$$u=u(x,y)\ ;\quad v=v(x,y) \tag{4.1}$$

and (2) the specified boundary tractions, T_{Sx} and T_{Sy}, in the x- and y-directions, respectively,

$$\begin{Bmatrix}T_{Sx}\\ T_{Sy}\end{Bmatrix}=\begin{bmatrix}\sigma_{xx} & \sigma_{xy}\\ \sigma_{xy} & \sigma_{yy}\end{bmatrix}\begin{Bmatrix}n_x\\ n_y\end{Bmatrix} \tag{4.2}$$

where n_x and n_y are direction cosines of the unit vector normal to the boundary.

2.2 Nodeless variable flux-based finite element formulation

A flux-based formulation [8] is implemented to derive the corresponding finite element equations for a nodeless variable structural finite element. For the triangular element shape, the distribution of displacements over the element in the x- and y-directions is assumed in the form,

$$u(x,y)=\sum_{i=1}^{6}N_i(x,y)u_i(t)=\lfloor N(x,y)\rfloor\ \{u\} \tag{5.1}$$

$$v(x,y)=\sum_{i=1}^{6}N_i(x,y)v_i(t)=\lfloor N(x,y)\rfloor\ \{v\} \tag{5.2}$$

where $\lfloor N(x,y)\rfloor$ consists of the element interpolation functions; $\{u\}$ and $\{v\}$ are the vectors of the unknown displacements and the nodeless variables. The nodeless variable interpolation functions implemented in this paper are,

$$N_4=L_2L_3\ ;\quad N_5=L_1L_3\ ;\quad N_6=L_1L_2 \tag{6}$$

Each nodeless variable interpolation function varies quadratically along one edge and vanishes along the other edges as highlighted by an example of N_6 in Fig. 1. To derive the finite element matrices using the flux-based formulation, the method of weighted residuals is first applied to Eq. (1),

$$\int_{\Omega}N_i\left(\frac{\partial\{E_S\}}{\partial x}+\frac{\partial\{F_S\}}{\partial y}\right)d\Omega=0 \tag{7}$$

where Ω is the element domain. Gauss's theorem is then applied to the flux derivative terms to yield,

$$\int_{\Omega}N_i\frac{\partial\{E_S\}}{\partial x}d\Omega=\int_{S}N_i\{E_S\}n_x d\Gamma-\int_{\Omega}\frac{\partial N_i}{\partial x}\{E_S\}d\Omega \tag{8}$$

$$\int_{\Omega}N_i\frac{\partial\{F_S\}}{\partial y}d\Omega=\int_{S}N_i\{F_S\}n_y d\Gamma-\int_{\Omega}\frac{\partial N_i}{\partial y}\{F_S\}d\Omega \tag{9}$$

where S is the element boundary. Substituting Eqs. (8)-(9) into Eq. (7) to yield,

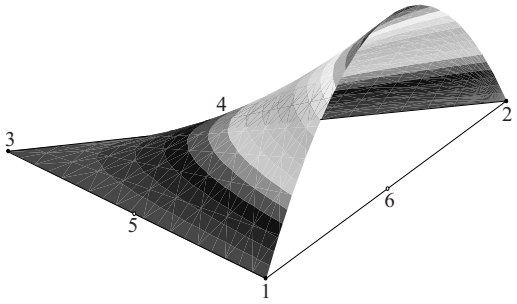

Fig. 1. An example of N_6 interpolation function for a typical triangular element.

$$\int_{\Omega}\frac{\partial N_i}{\partial x}\{E_S\}d\Omega+\int_{\Omega}\frac{\partial N_i}{\partial y}\{F_S\}d\Omega = \int_{S}N_i\{E_S\}n_x d\Gamma+\int_{S}N_i\{F_S\}n_y d\Gamma \tag{10}$$

The compact form of Eq. (10) can be written as,

$$\int_{\Omega}[B_S]^T\{\sigma\}d\Omega=\int_{S}[N]^T\{T_S\}d\Gamma \tag{11}$$

where

$$[B_S]=\begin{bmatrix}\frac{\partial N_1}{\partial x} & 0 & \cdots & \frac{\partial N_6}{\partial x} & 0\\ 0 & \frac{\partial N_1}{\partial y} & \cdots & 0 & \frac{\partial N_6}{\partial y}\\ \frac{\partial N_1}{\partial y} & \frac{\partial N_1}{\partial x} & \cdots & \frac{\partial N_6}{\partial y} & \frac{\partial N_6}{\partial x}\end{bmatrix}^T \tag{12.1}$$

$$[N]=\begin{bmatrix}N_1 & 0 & \cdots & N_6 & 0\\ 0 & N_1 & \cdots & 0 & N_6\end{bmatrix} \tag{12.2}$$

$$\{\sigma\}=\begin{bmatrix}\sigma_{xx} & \sigma_{yy} & \sigma_{xy}\end{bmatrix}^T \tag{12.3}$$

$$\{T_S\}=\begin{bmatrix}T_x & T_y\end{bmatrix}^T \tag{12.4}$$

In the flux-based formulation, the element flux distributions are computed from the nodal fluxes as,

$$\{\sigma\}=[\bar{N}]\{\bar{\sigma}\} \tag{13}$$

where

$$[\bar{N}]=\begin{bmatrix}\{\bar{N}\}^T & \{\bar{0}\}^T & \{\bar{0}\}^T\\ \{\bar{0}\}^T & \{\bar{N}\}^T & \{\bar{0}\}^T\\ \{\bar{0}\}^T & \{\bar{0}\}^T & \{\bar{N}\}^T\end{bmatrix} \tag{14.1}$$

$$\{\bar{\sigma}\}=\begin{Bmatrix}\{\sigma_{xx}\}_{1,2,3}\\ \{\sigma_{yy}\}_{1,2,3}\\ \{\sigma_{xy}\}_{1,2,3}\end{Bmatrix} \tag{14.2}$$

and the vectors $\{\bar{N}\}^T$ and $\{\bar{0}\}^T$ are

$$\{\bar{N}\}^T=\begin{bmatrix}N_1 & N_3 & N_3\end{bmatrix} \tag{15.1}$$

$$\{\bar{0}\}^T=\begin{bmatrix}0 & 0 & 0\end{bmatrix} \tag{15.2}$$

By following the same idea, the boundary tractions $\{T_S\}$ can be written as,

$$\{T_S\}=[\bar{N}]\{\bar{T}_S\} \tag{16}$$

where $[\bar{N}]$ and $\{\bar{T}_S\}$ are interpolation matrix and boundary tractions vector defined at the element boundary, respectively. The interpolation functions in Eq. (16) needed for integration along the element side *S* are,

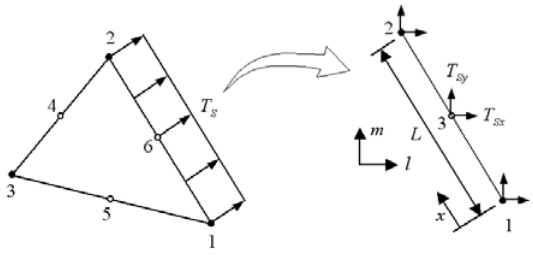

Fig. 2. Discretization of boundary tractions into the actual nodes and the nodeless variable on a typical element edge.

$$N_1=1-\frac{x}{L}\ ;\ N_2=\frac{x}{L}\ ;\ N_3=\frac{x}{L}\left(1-\frac{x}{L}\right) \tag{17}$$

where L is the length of element edge and x is the local coordinate along the edge starting from node 1 as shown in Fig. 2. Substituting Eqs. (13) and (16) into Eq. (11), the finite element equations for the element are,

$$\int_{\Omega}[B_S]^T[\bar{N}]d\Omega\{\bar{\sigma}\}=\int_{S}[N]^T[\bar{N}]d\Gamma\{\bar{T}_S\} \tag{18}$$

Appropriate boundary conditions of the given problem are then applied. Two types of the boundary conditions considered herein are the specified displacements and the specified boundary tractions, as given by Eqs. (4.1) and (4.2), respectively. These boundary conditions are applied at nodes directly as performed in the conventional finite element method. Finally, the system equations are iteratively solved for the nodal displacements and the nodeless variables using the preconditioned conjugate gradients technique with an element-by-element approximation [10].

3. The stress recovery and mesh adaptation

The stress recovery technique employed herein for the nodeless variable finite element follows the idea proposed by Zienkiewicz and Zhu [9], the so-called superconvergent patch recovery procedure. The procedure is a stress smoothing technique that works over element patches surrounding each node. A smooth stress field over the element patch, σ^*, is defined by,

$$\sigma^* = \lfloor P \rfloor \{a\} \tag{19}$$

where $\{a\}$ contains the coordinates to be determined and $\lfloor P \rfloor = \lfloor 1 \quad x \quad y \quad x^2 \quad xy \quad y^2 \rfloor$ contains terms of polynomials. Upon using the minimization process, the set of the equations shown below is obtained,

$$\left(\sum_{i=1}^{m} \lfloor P \rfloor_i^T \lfloor P \rfloor_i \right) \{a\} = \sum_{i=1}^{m} \lfloor P \rfloor_i^T \sigma_i \tag{20}$$

where m is the number of sampling points in the patch.

A measure of the discretization error in the elastic problem is referred as the Z^2-error estimate which is measured in energy norm. The percentage relative error is defined by,

$$\eta = \frac{\|\mathbf{e}\|_E}{\|\mathbf{u}\|_E} \times 100 \tag{21}$$

where $\|\mathbf{e}\|_E$ is the error in the energy norm and $\|\mathbf{u}\|_E$ is energy norm of the solution.

The mesh adaptation procedure proposed by Phongthanapanich and Dechaumphai [5] is implemented in this paper to generate proper element sizes according to the solution behavior. The mesh adaptation procedure requires the solution error, such as η, for guiding the mesh refinement and the regeneration process. The technique was first designed for analyzing hyperbolic problems, and has been modified recently for solving both the elliptic as well as the parabolic problems. The mesh adaptation process is terminated when the value of η is less than 5%, which is reasonable for many engineering applications [11]. The proper element size required for the mesh adaptation procedure is determined by the procedure proposed by Zienkiewicz and Zhu [12].

4. Numerical examples

To evaluate the performance of the proposed procedure with the implementation of the adaptive meshing technique, two examples are presented: a large plate with a small circular hole subjected to unidirectional tensile load, and a short cantilever beam with a rigidly fixed side.

4.1 A large plate with a small circular hole subjected to unidirectional tensile load

A large plate with a small circular hole [11] subjected to unidirectional tensile load $\sigma_\infty = 1$ is shown in Fig. 3. The plane stress condition is assumed with the Poisson's ratio of 0.3. This problem is a well-known benchmark test case for which the exact stress solutions are,

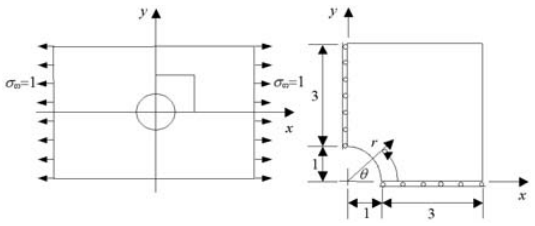

(a) (b)

Fig. 3. A large plate with a small circular hole subjected to unidirectional tensile load: (a) problem statement, (b) computational domain.

$$\begin{aligned}
\sigma_{xx} &= 1 - \frac{a^2}{r^2}\left(\frac{3}{2}\cos 2\theta + \cos 4\theta\right) + \frac{3}{2}\frac{a^4}{r^4}\cos 4\theta \\
\sigma_{yy} &= -\frac{a^2}{r^2}\left(\frac{1}{2}\cos 2\theta - \cos 4\theta\right) - \frac{3}{2}\frac{a^4}{r^4}\cos 4\theta \\
\sigma_{xy} &= -\frac{a^2}{r^2}\left(\frac{1}{2}\sin 2\theta + \sin 4\theta\right) + \frac{3}{2}\frac{a^4}{r^4}\cos 4\theta
\end{aligned} \tag{22}$$

where a is a radius of the hole, and (r, θ) are the polar coordinates.

The structured (S1, S2 and S3) and unstructured (U1 and U2) meshes, as shown in Fig. 4, are used in the finite element analysis for the stress solutions. The example is also used to evaluate the performance of the nodeless variable formulation on the structured *h*-refinement meshes and on the adaptive unstructured meshes. In this example, the first unstructured mesh U1 has a high percentage relative error of $\eta = 7.53\%$, which indicates the need for further mesh refinement. After only one adaptive meshing step, the unstructured mesh U2 is obtained with an acceptable value of $\eta = 1.00\%$. This second unstructured mesh U2 consists of 168 nodes and produces only 5% error as compared to the exact solution. Figs. 5(a)-(c) show the stress solutions σ_{xx}, σ_{yy}, and σ_{xy} along the radius $r = a$ obtained from the different meshes as compared to the exact solution. The figures show that nodeless variable elements on adaptive meshes can provide accurate stress solutions with fewer elements as compared to the others. The figure also highlights the oscillated stress distribution that is normally produced from the use of the standard constant strain triangle (CST) finite elements. More realistic stress distributions are obtained from the nodeless variable ele-

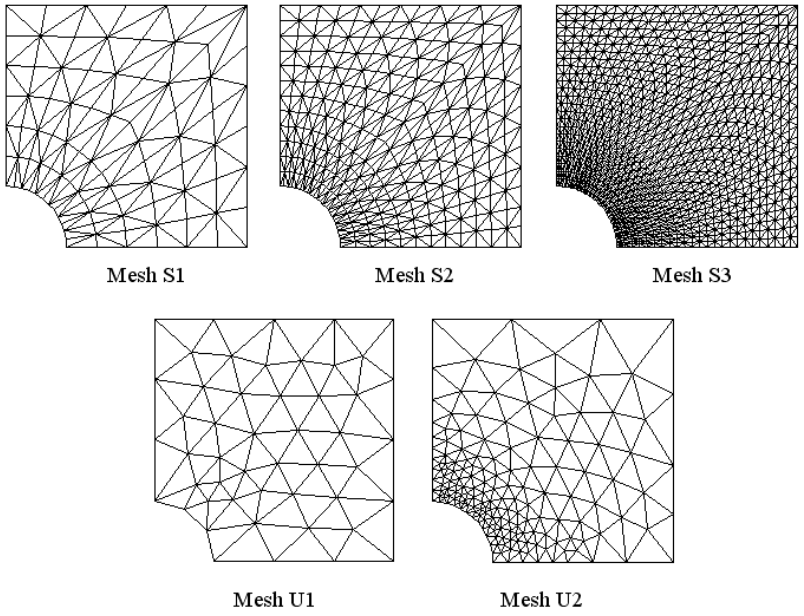

Fig. 4. Meshes used in the analysis of plate with circular hole.

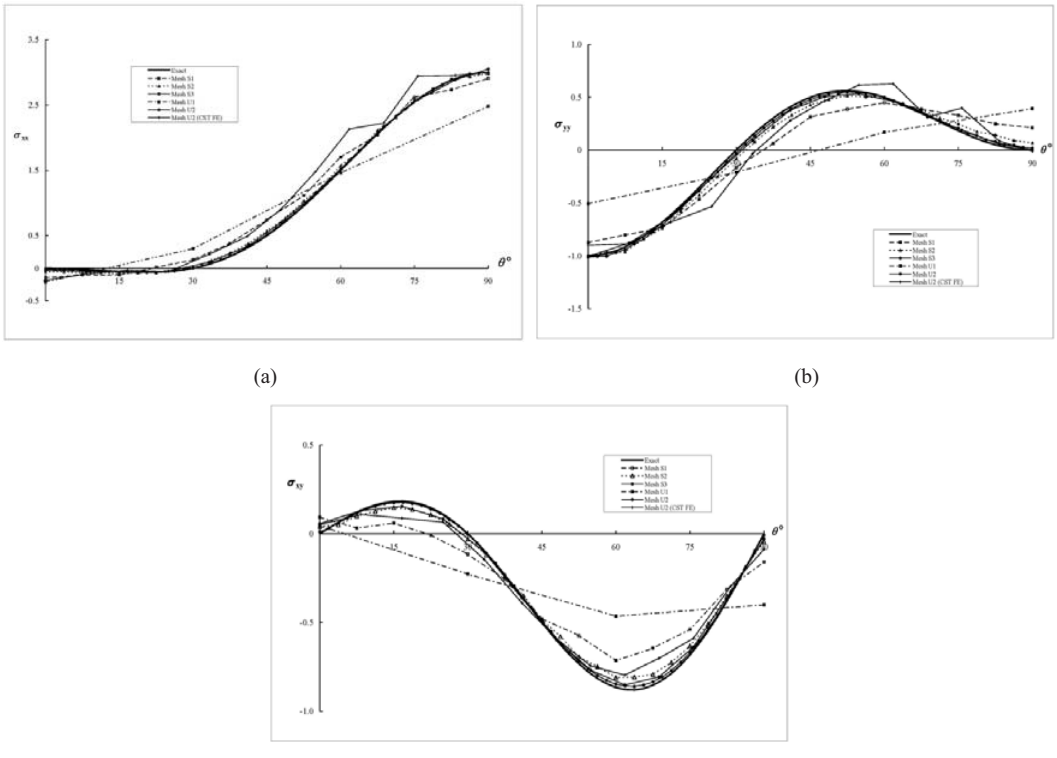

Fig. 5. Comparison of stresses along $r = a$ for plate with circular hole: (a) σ_{xx}, (b) σ_{yy}, and (c) σ_{xy} (nodeless and CST FEs).

ments by the implementation of the stress recovery process. Figs. 6(a)-(c) show a comparison of the stress solutions obtained from using a nodeless variable and the standard 6-node triangular elements

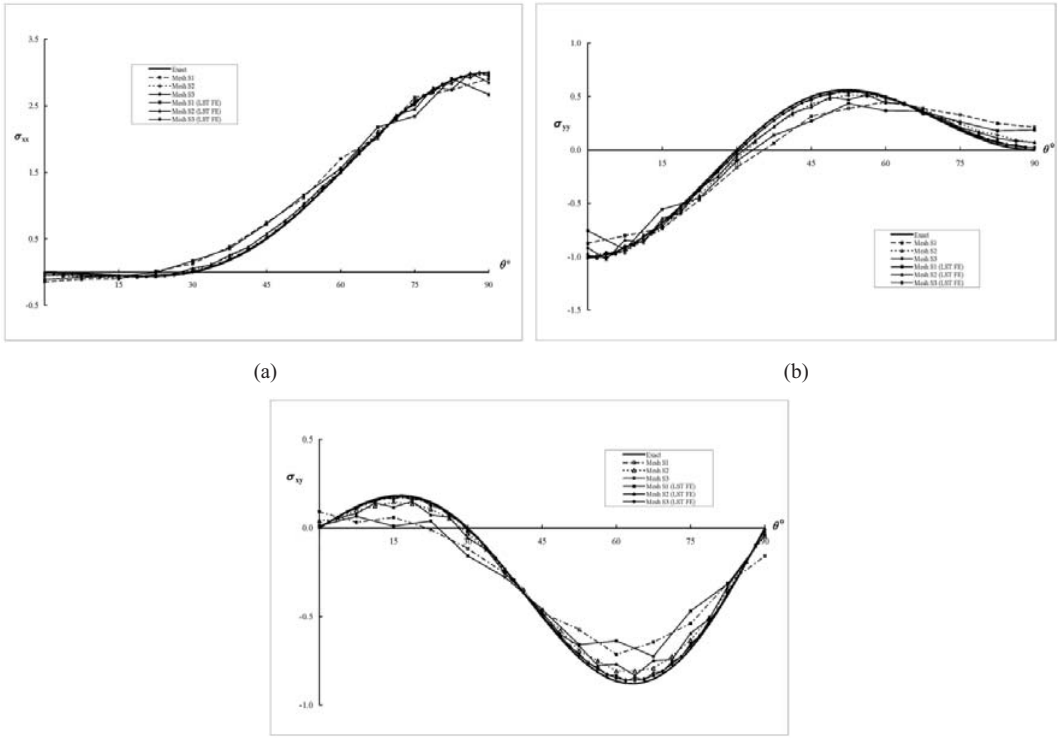

(a) (b)

(c)

Fig. 6. Comparison of stresses along $r = a$ for plate with circular hole: (a) σ_{xx}, (b) σ_{yy}, and (c) σ_{xy} (nodeless and LST FEs).

	η		Number of iterations	
Mesh	Nodeless	LST	Nodeless	LST
S1	8.32	7.96	172	253
S2	6.48	6.34	305	539
S3	4.50	4.48	587	1018

Fig. 7. Comparison of the percentage relative errors and the number of iterations for example of plate with circular hole.

(linear strain triangle-LST) on the three structured meshes. The computed percentage relative errors and the number of iterations to achieve the error level of 10^{-10} (L_2 norm error measurement) are shown as a table in Fig. 7. The solution accuracy obtained from the two methods is comparable. However, the number of iterations used by the nodeless variable method for solving the system equations is almost a half fewer than that used by the conventional method with the LST elements.

4.2 A short cantilever beam with a rigidly fixed side

The second test case is a short cantilever beam with a rigidly fixed side subjected to a compressive load of

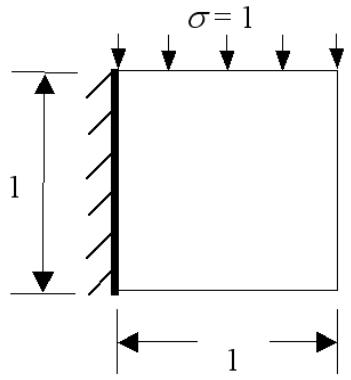

Fig. 8. Problem statement of a short cantilever beam with a rigidly fixed side.

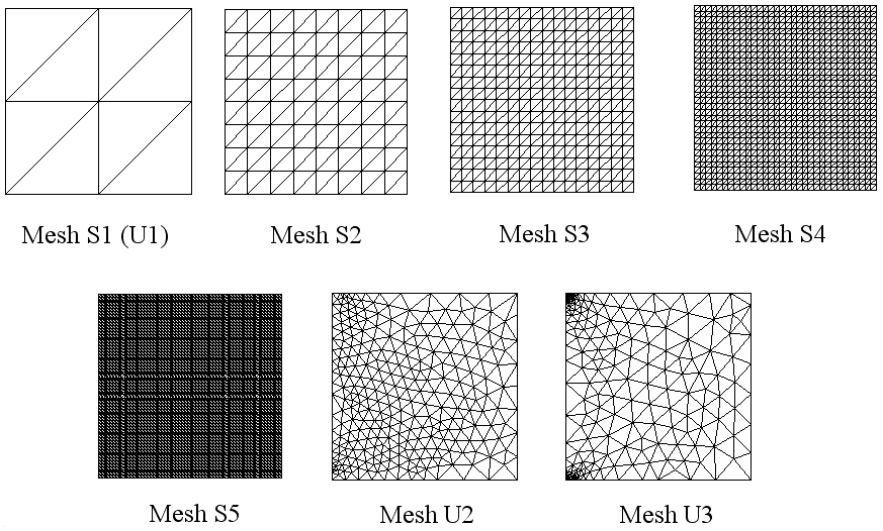

Fig. 9. Meshes used in the analysis of short beam example.

Mesh	Number of nodes	η
S1 (U1)	9	23.96
S2	81	7.91
S3	289	4.73
S4	1089	2.87
S5	4225	1.75
U2	273	3.66
U3	286	1.55

Fig. 10. Comparison of the percentage relative errors for a short beam example.

	η		Number of iterations	
Mesh	Nodeless	LST	Nodeless	LST
S1	23.96	16.81	44	44
S2	7.91	5.77	127	225
S3	4.73	3.48	233	450
S4	2.87	2.12	457	891
S5	1.75	1.29	891	1760

Fig. 11. Comparison of the percentage relative errors and the number of iterations for a short beam example.

σ = 1 [11] as shown in Fig. 8. The plane strain condition is assumed with the Poisson ratio of 0.3. Fig. 9 shows the five uniform meshes (S1 to S5) and the two adaptive meshes (U2 and U3) used in the finite element analysis. The table in Fig. 10 shows the numbers of nodes in different meshes, as well as their computed percentage relative errors. The table also indicates that, by starting from the uniform mesh (S1), a relative error of less than 5% is achieved with only one adaptive step (U2, 273 nodes and η = 3.66%). Their computed percentage relative errors and the number of iterations to achieve the error level of 10^{-10} are shown as a table in Fig. 11. The accuracy of the solutions obtained by using the LST elements is slightly better than the nodeless variable elements; however, the difference becomes smaller when the mesh is refined. Similar to the previous example, the nodeless variable method converges approximately twice faster than the conventional finite element method with the LST elements.

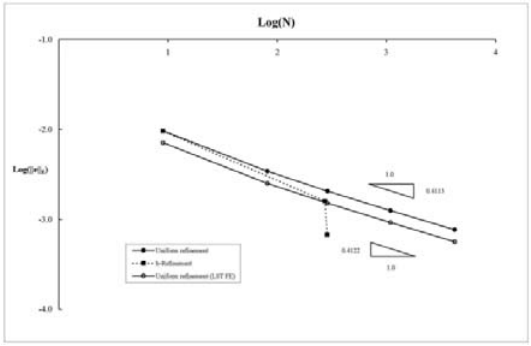

Fig. 12. Comparison of solution convergences between uniform refinement and adaptive meshes used in the short beam example.

The solution convergence rates between the uniform refinement meshes and the adaptive meshes are also presented in Fig. 12. The converge rates of all uniform refinement meshes are relatively low due to the solution singularity at the lower and upper left

corners. Numerical experiment also suggests that the nodeless variable method still performs well to provide high solution accuracy on the adaptive meshes as compared to the uniform meshes.

5. Conclusion

The nodeless variable flux-based finite element method was developed to analyze two-dimensional elasticity problems. The flux-based formulation was applied to reduce the computational complexity as compared to the conventional finite element method. The rate of the solution convergence was improved by combining the method with an adaptive meshing technique. The superconvergence patch recovery procedure was also modified and implemented for the nodeless variable element. The performance of the combined procedure was evaluated by two benchmark examples. The examples demonstrated the efficiency of the proposed method for providing accurate solutions with rapid convergence rates as compared to the conventional finite element method.

Acknowledgment

The authors are pleased to acknowledge the Thailand Research Fund (TRF) for supporting this research work.

References

[1] P. J. Heyes, M. G. Milsted and J. Dakin, Multiaxial fatigue assessment of automotive chassis components on the basis of finite element models, 4th International Conference on Biaxial/Multiaxial Fatigue, Saint-Germain en Laye, France, (1994).

[2] W. Limtrakarn and P. Dechaumphai, Interaction of high-speed compressible viscous flow and structure by adaptive finite element method, *KSME Int. J*. 18 (10) (2004) 1837-1848.

[3] A. K. Noor, Computational structures technology: leap-frogging into the twenty-first century, *Comput. & Structures*. 73 (1) (1999) 1-31.

[4] H. Z. Tang and T. Tang, Adaptive mesh methods for one- and two-dimensional hyperbolic conservation laws, *SIAM J. Numer. Anal*. 41 (2) (2003) 487-515.

[5] S. Phongthanapanich and P. Dechaumphai, Two-dimensional adaptive mesh generation algorithm and its application with higher-order compressible flow solver, *KSME Int. J*. 18 (12) (2004) 2190-2203.

[6] J. E. Tarancon, F. J. Fuenmayor and L. Baeza, An a posteriori error estimator for the *p*- and *hp*-versions of the finite element method, *Int. J. Numer. Methods Eng.* 62 (1) (2005) 1-18.

[7] O. C. Zienkiewicz, The background of error estimation and adaptivity in finite element computations, *Comput. Meths. Appl. Mech. Engrg.* 195 (4-6) (2006) 207-213.

[8] S. Phongthanapanich, S. Traivivatana, P. Boonmaruth and P. Dechaumphai, Nodeless variable finite element method for heat transfer analysis by means of flux-based formulation and mesh adaptation, *Acta Mech. Sin*. 22 (2) (2006) 138-147.

[9] O. C. Zienkiewicz and J. Z. Zhu, The superconvergent patch recovery and a posteriori error estimates. part 1: the recovery technique, *Int. J. Numer. Methods Eng*. 33 (7) (1992) 1331-1364.

[10] T. J. R. Hughes, I. Levit and J. Winget, An element-by-element solution algorithm for problems of structural and solid mechanics, *Comput. Meths. Appl. Mech. Engrg*. 36 (2) (1983) 241-254.

[11] O. C. Zienkiewicz and R. L. Taylor, The finite element method. volume 1: the basis, 5th Edition, Butterworth-Heinemann, Woburn, (2000).

[12] O. C. Zienkiewicz and J. Z. Zhu, Adaptivity and mesh generation, *Int. J. Numer. Methods Eng*. 32 (4) (1991) 783-810.